

Stochastic Hydro-thermal Unit Commitment via Multi-level Scenario Trees and Bundle Regularization

E. C. Finardi ^{*} R. D. Lobato [†] V. L. de Matos [‡] C. Sagastizábal [§]
A. Tomasgard [¶]

April 15, 2019

Abstract

For an electric power mix subject to uncertainty, the stochastic unit-commitment problem finds short-term optimal generation schedules that satisfy several system-wide constraints. In regulated electricity markets, this very practical and important problem is used by the system operator to decide when each unit is to be started or stopped, and to define how to generate enough energy to meet the load. For hydro-dominated systems, an accurate description of the hydro-production function involves non-convex relations. This feature, combined with the fine time discretization needed to represent uncertainty of renewable generation, yields a large-scale mathematical optimization model that is nonlinear and has mixed-integer variables. To make the problem tractable, a novel solution strategy, based on multi-horizon scenario trees, is proposed. The approach deals in a first level with the integer decision variables representing whether units are on or off. Once units are committed, the expected operational cost is minimized by solving a continuous second-level problem, which is separable by scenarios. The coordination between the two decision levels is done by means of a bundle-like variant of Benders decomposition that proves very efficient for the considered setting. To assess the quality of the optimal commitment on out-of-sample scenarios, a new simulation technique, based on certain sustainable pseudo-distance is proposed. For the numerical experiments, a mix of hydro, thermal, and wind power plants extracted from the Brazilian power system is considered. The results confirm the interest of the approach, particularly regarding a more efficient management of hydro-plants, because non-convex operational regions are considered by the model.

^{*}Laboratório de Planejamento de Sistemas de Energia Elétrica, Universidade Federal de Santa Catarina. Email: erlon.finardi@ufsc.br.

[†]Department of Applied Mathematics, Institute of Mathematics, Statistics, and Scientific Computing, State University of Campinas (IMECC - UNICAMP), Rua Sérgio Buarque de Holanda 651, 13083-859, Campinas, SP, Brazil. E-mail: lobato@ime.usp.br. Research of this author is supported by FAPESP grants 2015/18053-9 and 2017/05198-4.

[‡]Plan4 Engenharia. Email: vitor@plan4.com.br.

[§]Adjunct Researcher IMECC - UNICAMP. Email: sagastiz@unicamp.br. Research of this author is supported by CNPq Grant 303905/2015-8 and by CEMEAI.

[¶]Department of Industrial Economics and Technology Management, NTNU, Trondheim Norway. Email: asgeir.tomasgard@ntnu.no

AMS Subject Classification: Primary 90C15; Secondary 49M27.

Keywords: Unit Commitment; Stochastic Optimization; Multi-horizon Scenario Trees; Non-convex hydro-production function; Regularized Benders Decomposition; Bundle Methods.

1 Introduction and motivation

The unit-commitment (UC) problem determines the optimal scheduling of generating units over a short-term horizon, typically ranging between 24 and 168 hours, [WSL08; SF94]. In response to the increasing penetration of renewable energy, a variety of stochastic unit-commitment (SUC) models has been proposed in the literature, we refer to [Tah+15] for a thorough review. Most of the considered models handle uncertainty by scenario representation in a two-stage setting. For instance, in [PO13] the deterministic formulation [SS09] is extended so that in the first stage slow generators are committed; subsequently, once uncertainty in net demand and in availability of units and lines is revealed, the second-stage subproblems solve a dispatch problem to find optimal fast generator commitments and production schedules for each scenario; see also [PO12]. The more recent work [ZCS17] combines day-ahead UC decisions in the first stage with real-time dispatch and market-balancing decisions in the second stage.

The references above formulate the SUC problem in a deregulated market framework, with market-clearing constraints. We are interested in the Brazilian power system, with an independent system operator centralizing the decisions on generation, transmission and distribution of energy for the whole country. Accordingly, Brazil's SUC model minimizes the expected cost of a very large hydro-dominated configuration, with water travel times of one week in some regions. In this context wind farms and run-of-river plants, with their intermittent generation, significantly complicate the optimization problem. The reason lies in the disparity between the fine time discretization needed for the uncertainty and the long time horizon (at least one week) that must be considered to take into account coupling constraints involving hydro-valleys.

The hydro-production function (HPF), that converts turbined outflow into energy, complicates even more the optimization problem. Namely, a satisfactory model of the HPF introduces a non-convex equality in the feasible set, see Sections 2.1 and 5.1. Given that the SUC models are run every day, providing an output in less than 90-120 minutes for operational purposes, the Brazilian SUC problem constitutes a true challenge from the solution point of view.

In such a setting, integrating renewable power and its uncertainty in a manner that is sound and accurate is crucial. A multi-stage stochastic programming model for large-scale mixed-integer non-convex problems is out of reach with the current computational capabilities. On the other hand, the two-stage paradigm has some drawbacks; for instance, in some situations it is not sufficient to look at just one stage ahead, as it happens when uncertainty is revealed all at once, for the whole week (two-stage UC models cannot adapt generation schedules and dispatch to hourly uncertainty realizations). We propose a novel model based on the concept of multi-horizon scenario tree. The idea is to work with two separate groups of variables, called strategic and operational. The strategic group, corresponding to the first level decision, includes variables with a slow dynamic, like the on/off status of the units, which can change at most twice or thrice a day. The operational group, in turn, deals with continuous variables such as generation levels,

reservoir volumes, and network flows, that need to adapt to a fast dynamic (water inflow and wind). All 0-1 decisions are taken in the first level; in the second decision level, the 0-1 variables related to UC are fixed. Decision levels are coordinated by means of a bundle-like regularized Benders approach which maintains the 0-1 linear structure of the master program, but provides better bounds and, hence, converges faster than a classical Benders decomposition method.

The contribution of this work is three-fold. On the modeling side, differently from the two-stage paradigm in [PO13; PO12; ZCS17], multi-horizon trees make it possible to consider uncertainty in both decision levels. However, multi-horizon trees, as introduced in [Kau+14], are not applicable straightforwardly because our SUC problem has ramp constraints and water balance equations coupling several time steps (the problem structure in [Kau+14] does not present any temporal coupling). Instead, we combine a tree on the strategic decision level with a fan of independent scenarios in the operational level. The advantage over classical two-stage models is that the on/off status of the units can change and react to variations in the demand throughout the day. This flexibility, crucial to reduce costs, is closer to real-time operation conditions, and is best exploited when the system under consideration has many units with fast operational dynamics, such as hydro-units and some thermal gas turbines. Furthermore, being an intermediate representation between two- and multi-stage formulations, the multi-horizon paradigm does not suffer from the dimensionality curse typical of multi-stage scenario trees.

The second area of contribution of this work is on the methodological side. Our regularized method stabilizes the pure Benders algorithm, preventing oscillations and tailing-off effects that slow down the iterative process and sometimes impair convergence. Our bundle-like decomposition method, could be seen as an enhancement of [LTB11], which is based on the Generalized Benders Decomposition (GBD) [Geo72]. To ensure convergence, such decomposition methods solve a master program and slave problems to define lower and upper bounds that are refined along iterations. Since there are non-convex constraints in the slave problems, the upper bound computes global solutions to nonlinear programs, a process which [LTB11] reports to take 90% of the total running time. An interesting feature regarding UC is that, unlike methods based on Lagrangian relaxation, Benders'-like algorithms output feasible schedules directly, without any need of *a posteriori* heuristic phases to recover primal feasibility, even with a non-convex HPF.

Finally, the third contribution refers to how the quality of the SUC solution is assessed, a crucial feature in stochastic programming. We introduce a new simulation procedure that, given the optimal commitment for the in-sample scenarios and a set of out-of-sample scenarios, finds the closest commitment in terms of certain *sustainable pseudo-distance* similar to the well-known Fortet-Mourier distance, but weighed so that wind energy is best used.

The work is organized as follows. The problem to be solved is formulated in Section 2; subsections 2.1 and 2.2 therein present, respectively, the structure of the UC problem under consideration and several concepts associated with multi-horizon scenario trees. Section 3 explains the main elements of the solution methodology, combining the non-convex Generalized Benders decomposition with a bundle-like regularization. Section 4 provides several implementational issues, such as the approximation procedure of the HPF and the new simulation technique. Section 5 details the SUC formulation for a hydro-thermal configuration extracted from the Brazilian power system and assesses the numerical performance of our proposal under different conditions. A final section with the main conclusions ends the paper.

Notation. All vectors are considered column vectors. Given two vectors x, \tilde{x} , their Euclidean inner product is $\langle x, \tilde{x} \rangle = x^\top \tilde{x}$. Time steps are denoted by a subindex $t \in \{1, 2, \dots, \mathbb{T}\}$, where \mathbb{T} is the time horizon. The rest of the notation is introduced gradually, starting with the SUC problem description in the next section.

2 Problem formulation

To ease the presentation, the main elements of the problem are given first for a deterministic model. Uncertainty is taken into account later on, when explaining the multi-horizon trees in subsection 2.2.

2.1 The unit-commitment model

Decision variables are split into two vectors, x and y , respectively with 0-1 and continuous components. If the i th unit is on at time t , the variable x_t^i is set to 1, otherwise is equal to 0. Scalars y_t^i correspond to decisions related to operation: turbined outflow, spillage, unit generation, line flows, and voltage angles. Transmission in the electrical system is represented by DC affine relations between buses and lines. Operational decision variables of all the units at time t are denoted by y_t . In particular, an important subvector is the energy generated by the whole system at time t , denoted by g_t , with values ranging in the (multi-dimensional) interval $[\gamma, \Gamma]$, the same for all t . **When a unit is switched on or immediately before it is switched off, it is assumed to generate the minimum power γ .** Ramps have up and down-rates δ^+ and δ^- , defining the parameters $\rho^+ := \delta^+ - \gamma$ and $\rho^- := \delta^- - \gamma$. Decisions on commitment (operation) are taken at the beginning (end) of a time period.

The abstract formulation below gives the general structure of the UC problem, the rightmost text, between parentheses, explains the meaning of each set of constraints.

$$\left\{ \begin{array}{ll} \min & \sum_{t=1}^{\mathbb{T}} (\langle \mathcal{F}_t, x_t \rangle + f_t(y_t)) \\ \text{s.t.} & x_t^i \in \{0, 1\}, y_t^i \geq 0 \quad \text{for all } i, t \\ & A_t^0 y_{t-1} + A_t^1 y_t = a_t \quad \text{for all } t \quad (\text{water balance}) \\ & B_t y_t = b_t \quad \text{for all } t \quad (\text{power balance on each bus}) \\ & C_t y_t \leq c_t \quad \text{for all } t \quad (\text{transmission lines}) \\ & g_{t-1} - g_t \leq \gamma + \rho^- x_t \quad \text{for all } t \quad (\text{down-ramp}) \\ & g_t - g_{t-1} \leq \gamma + \rho^+ x_{t-1} \quad \text{for all } t \quad (\text{up-ramp}) \\ & x_t \gamma \leq g_t \leq x_t \Gamma \quad \text{for all } t \quad (\text{generate only for switched-on units}) \\ & E g_t = \text{hp}(y_t) \quad \text{for all } t \quad (\text{hydro-production function}). \end{array} \right. \quad (1)$$

In the objective function, the linear commitment costs \mathcal{F}_t are related to the cost incurred when starting up and shutting down a unit. Operational costs are represented by the function f_t , which can be linear, piecewise-linear or quadratic convex. Typically, thermal generation has linear or quadratic convex costs, and the cost of hydro-generation is given by a piecewise-linear function. Matrices and vectors in the feasible set have suitable dimensions. **An observation regarding the water balance constraint is in order. At first sight, its formulation does not appear to take into**

account the *water travel time* between two hydro-plants in cascade. When the time that takes for outflows upstream to reach the reservoir downstream is longer than one discretized unit of time, the water balance constraint couples variables from times earlier than $t-1$. Notwithstanding, the format presented in (1) remains valid, simply by adding auxiliary non-negative variables that accumulate consecutive portions of the water travel time (incidentally, such auxiliary variables must satisfy relations akin to the one given for the water balance, that is, coupling $t-1$ and t).

A more compact problem formulation, handy for explaining both the multi-horizon trees and the decomposition method, makes use of the sets

$$\mathcal{Y}_t := \{y_t \in \mathbb{R} \mid A_t^0 y_{t-1} + A_t^1 y_t = a_t, D_t^0 y_{t-1} + D_t^1 y_t \leq d_t\} \quad (2)$$

which couple decisions on consecutive time steps, and the static constraint sets,

$$\mathcal{X}_t := \{x_t \in \{0, 1\}\}, \quad \text{and} \quad \mathcal{S}_t := \{y_t \geq 0 \mid B_t y_t = d_t, E g_t = \text{hp}(y_t)\}, \quad (3)$$

to be satisfied separately by x or y , only for components with sub-index t .

With this notation, problem (1) writes down as follows

$$\begin{cases} \min & \langle \mathcal{F}, x \rangle + f(y) \\ \text{s.t.} & x_t \in \mathcal{X}_t, y_t \in \mathcal{S}_t \cap \mathcal{Y}_t \text{ for all } t \\ & T x + W y \leq h, \end{cases} \quad (4)$$

where the inequality constraint represents the ramps and the bounds on capacity $x_t \gamma \leq g_t \leq x_t \Gamma$, coupling some components of x and y at each time step.

2.2 Information structure, uncertainty and decisions

In problem (4), uncertainty appears in the right-hand side terms b and d to represent the impact of unknown inflows and wind generation on, respectively, the water and power balance equations. Letting the corresponding random data process be ξ_t , its history up to time t is denoted by $\xi_{[t]}$, assuming that ξ_1 is deterministic. Regarding (4), we now have that $\mathcal{S}_t = \mathcal{S}_t(\xi_t)$ depends only on the t -th realization. By contrast, the sets

$$\mathcal{X}_t = \mathcal{X}_t(\xi_{[t]}) \quad \text{and} \quad \mathcal{Y}_t = \mathcal{Y}_t(\xi_{[t]}) \quad (5)$$

depend on the whole history, because the ramps couple x_{t-1} and x_t with y_{t-1} and y_t . This is an important issue, that prevents a straightforward application of the multi-horizon trees in [Kau+14]. In these work the feasible sets are stagewise independent. By contrast, with our setting decision variables become a function of the uncertainty history, for each t

$x := (x_1, x_2(\xi_{[2]}), \dots, x_{\mathbb{T}}(\xi_{[\mathbb{T}]}))$ and, similarly for the operational constraints.

A risk-neutral multi-stage stochastic programming version of the problem is

$$\begin{cases} \min & \mathbb{E}_\xi [\langle \mathcal{F}, x(\xi) \rangle + f(y(\xi))] \\ \text{s.t.} & x_t(\xi_{[t]}) \in \mathcal{X}_t(\xi_{[t]}) & \text{for a.e. } \xi, \text{ for all } t \\ & y_t(\xi_{[t]}) \in \mathcal{S}_t(\xi_t) \cap \mathcal{Y}_t(\xi_t) & \text{for a.e. } \xi, \text{ for all } t \\ & T x(\xi_{[\mathbb{T}]}) + W y(\xi_{[\mathbb{T}]}) \leq h & \text{for a.e. } \xi. \end{cases} \quad (6)$$

Suppose the data process distribution is finite, given by scenarios $\xi_{[\mathbb{T}]}^1, \xi_{[\mathbb{T}]}^2, \xi_{[\mathbb{T}]}^3, \dots$. With a multi-horizon tree structure, the process attached to the strategic variable x can be handled differently from the one attached to the operational variable y . For this reason, we write separately the uncertainty for x and y , as follows:

$$\begin{cases} \min & \mathbb{E}_\omega [\langle \mathcal{F}, x(\omega) \rangle] + \mathbb{E}_\xi [f(y(\xi))] \\ \text{s.t.} & x_t(\omega_{[t]}) \in \mathcal{X}_t(\omega_{[t]}) & \text{for all } t \\ & y_t(\xi_{[t]}) \in \mathcal{S}_t(\xi_t) \cap \mathcal{Y}_t(\xi_t) & \text{for all } t \\ & Tx(\omega_{[\mathbb{T}]}) + Wy(\xi_{[\mathbb{T}]}) \leq h, \end{cases}$$

where the relations hold for almost every ω and ξ . Clearly, if $\omega_t = \xi_t$ for all t , the problem above is equivalent to (6). Notwithstanding, nothing prevents from choosing different scenarios for each data process, to the extent that the strategic tree, representing ω , can branch at time steps that are *different* from those in the operational tree, representing ξ . Such a distinction is well suited to our setting: as changes in commitment (x) have a slow dynamic, it is sound to branch in blocks of a few hours (i.e., 4, 8, etc.), to modify the unit status at most a given number of times a day. Operation decisions (y), by contrast, should adapt to the fast dynamic of wind realizations and branching every hour makes better sense. In this case, strategic scenarios have length $|\mathbb{T}|^x$ while operational ones have length $|\mathbb{T}|^y$.

In a traditional scenario tree for multi-stage recourse problems [KW94], combining a slow dynamic for x with a fast dynamic for y rapidly grows out of hand and is bound to the well-known dimensionality curse. Two-stage approaches, on the other hand, are not sufficiently flexible in terms of recourse, particularly when it comes to switch on and off units to adapt generation (and ramps) to wind power changes.

There is one important issue that arises at this point, related to the use of separate time scales. When branching at different paces in both trees, the coupling constraint

$$Tx(\omega_{[\mathbb{T}^x]}) + Wy(\xi_{[\mathbb{T}^y]}) \leq h,$$

needs to be defined by suitably *linking* scenarios in both trees. This is done by means of an application denoted by ν , linking nodes in the strategic and operational trees. The constraint is then replaced by

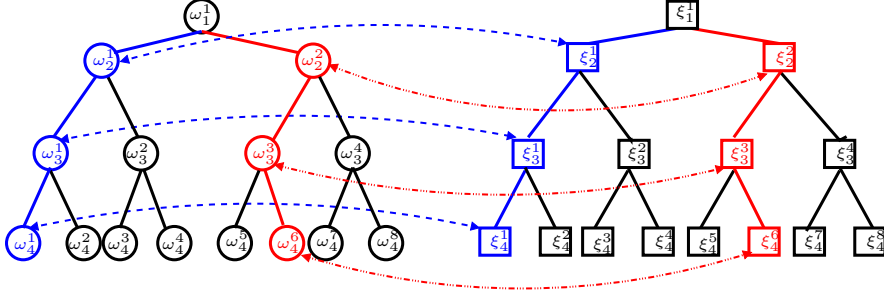
$$Tx(\omega_{[\nu(\mathbb{T}^y, \xi)]}) + Wy(\xi_{[\mathbb{T}^y]}) \leq h.$$

In order to better explain how nodes in the trees are connected, we illustrate in Figures 1, 2 and 3 some situations that may arise, assuming that at most two realizations can occur for the data processes. Circles and squares are used in the figures to represent scenario nodes generated for the distribution of ω and ξ , respectively.

The two multi-stage trees in Figure 1 have the same time scale $|\mathbb{T}|^x = |\mathbb{T}|^y = 4$. The strategic tree for the decision variable x on the left has nodes represented as circles. On the right-hand side tree the square nodes correspond to the operational variable, y . There is clear a one-to-one relation; the corresponding mapping ν is represented by the (dash and dash-dot) lines joining circles and squares in the figure.

The situation changes when using different time scales. Suppose the strategic tree (with slow dynamic) does not branch at $t = 2$, as in the left tree in Figure 2, where $|\mathbb{T}|^x = 3$ and $|\mathbb{T}|^y = 4$.

Figure 1: One-to-one link for multi-horizon trees with same time scales.

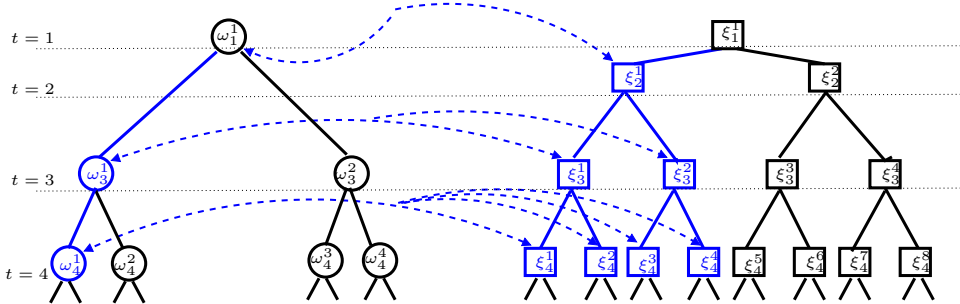


Lacking nodes for $t = 2$ on the left tree, the operational variables in nodes for $t = 2$ (squares labelled ξ_2^1 and ξ_2^2) are linked with the on/off status defined at $t = 1$ (circle labelled ω_1^1). In particular, for $\xi_{[2]} = (\xi_1^1, \xi_2^1)$ in the figure,

$$\begin{array}{l} \text{the capacity constraint } x_2(\omega_{[2]}) \quad \gamma \leq g_2(\xi_{[2]}) \leq x_2(\omega_{[2]}) \quad \Gamma \\ \text{is replaced by} \quad x_1 \quad \gamma \leq g_2(\xi_{[2]}) \leq x_1 \quad \Gamma. \end{array}$$

and similarly for $\xi_{[2]} = (\xi_1^1, \xi_2^1)$.

Figure 2: Many-to-many link for multi-horizon trees with different time scales.



Defining a nonanticipativity replacement for the ramp constraints

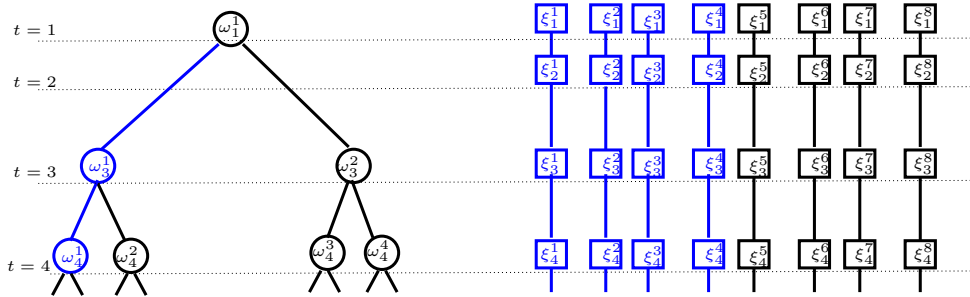
$$g_{t-1}(\xi_{[t-1]}) - g_t(\xi_{[t]}) \leq \gamma + \rho^- x_t(\omega_{[t]}) \quad \text{and} \quad g_t(\xi_{[t]}) - g_{t-1}(\xi_{[t-1]}) \leq \gamma + \rho^+ x_{t-1}(\omega_{[t-1]})$$

is more complicated. The property of nonanticipativity states that, in multi-stage trees, decisions sharing same uncertainty history must be the same. In the multi-horizon formulation [Kau+14] linking two time scales is simple, because therein constraints involving the two trees are not coupled in time and consistency is preserved in a straightforward manner. This is not the case for SUC problems with ramp constraints. To understand the difficulty, note that in Figure 2, nonanticipativity means that the strategic scenario $(\omega_1^1, \omega_3^1, \omega_4^1)$ is associated with the four leftmost operational scenarios

$$\xi_{[4]}^1 := (\xi_1^1, \xi_2^1, \xi_3^1, \xi_4^1), \xi_{[4]}^2 := (\xi_1^1, \xi_2^1, \xi_3^1, \xi_4^2), \xi_{[4]}^3 := (\xi_1^1, \xi_2^1, \xi_3^2, \xi_4^3), \text{ and } \xi_{[4]}^4 := (\xi_1^1, \xi_2^1, \xi_3^2, \xi_4^4). \quad (7)$$

Since one component of the operational uncertainty refers to inflows, the operational scenarios (7) can be thought of as representing four different reservoir dynamics, which are in turn associated with four different generation levels. On the strategic tree, scenarios represent different system configurations (commitments), determining the ramps and the generation capacity for each unit in the system. The inconsistency arises at $t = 5$, because the same four operational scenarios (7) are associated with the strategic scenario $(\omega_1^1, \omega_3^1, \omega_4^2)$. Since the realizations ω_4^1 and ω_4^2 are not the same, the corresponding different system configurations should lead to different generation decisions and yield different reservoir dynamics on the operational nodes after $t = 5$. Having different reservoir dynamics is clearly not possible on the same operational tree. On the other hand, if each strategic scenario had attached its own operational tree, the involved computational effort would make the model unpractical. For this reason, instead of representing operational uncertainty by a multi-stage tree, we drop the nonanticipativity requirement on the operational side and employ a fan of independent scenarios, as in Figure 3.

Figure 3: Multi-stage tree and fan of independent scenarios using different time scales.



When using a fan of independent scenarios for the operational uncertainty the generation decisions are taken separately for each scenario. This introduces an inconsistency in the decision process, because often scenarios are sampled so that they have a common history of realizations. To understand this issue, suppose the fan in Figure 3 has two inflow scenarios that coincide for the first three time steps. The corresponding generation decisions will be different, when in fact they should be the same for the first three time steps. This inconsistency in the operational level is the price to pay to have the possibility of representing uncertainty in the strategic variables. For the problem of interest, the most important output of the model is the commitment. The generation levels can be adjusted in real time by the operator, according to the realization of uncertainty. Once a unit is on, it is acceptable to modify slightly its generation. By contrast, especially in the presence of ramping constraints, it is crucial to make sure that a given unit is not switched-off at times close to peak demand or when there is a high probability of losing a significant amount of wind generation. These considerations are the main motivation for our modeling choice.

3 Decomposition method

Similarly to Section 2, to explain the methodology without carrying on a heavy notation, we consider the deterministic problem (4) with feasible sets from (2) and (3):

$$\begin{cases} \min & \langle \mathcal{F}, x \rangle + f(y) \\ \text{s.t.} & x_t \in \mathcal{X}_t, y_t \in \mathcal{S}_t \cap \mathcal{Y}_t \text{ for all } t \\ & Tx + Wy \leq h. \end{cases}$$

Recall that the only non-convex relation appears in the HPF constraint $Eg_t = \text{hp}(y_t)$, included in the set with static constraints, \mathcal{S}_t . The first two subsections below describe the main ingredients of our decomposition method, namely how to handle non-convexity and the bundle-like regularization. In the final subsection, we explain how the approach is applied to the SUC when the multi-horizon formulation represented in Figure 3 is employed.

3.1 Generalized Benders decomposition for non-convex problems

Non-convexity is dealt with as in [LTB11], taking advantage of the fact that HPFs have been considered in convex and non-convex formulations [GH05; DM08; SZ13; KCW18; FFM19]. More precisely, suppose the following approximation of the HPF is available:

$$\exists H \text{ such that } \text{hp}(y_t) \leq H(y_t) \text{ for all } y_t, \text{ with } H \text{ concave.} \quad (8)$$

The proposal in [LTB11] is to replace the non-convex constraint $Eg_t = \text{hp}(y_t)$ by the convex constraint $Eg_t \leq H(y_t)$, and perform a Benders decomposition on the convexified problem. Since (8) ensures that the convex feasible set is larger than the original one, solving the convexified problem provides a lower bound for the non-convex optimal value. Upper bounds are found by solving the non-convex problem (4) only on the continuous variables, with fixed commitment x . The pseudo-code for the method in [LTB11] is given in Algorithm 1.

Some comments regarding Algorithm 1 are in order. First, to generate Benders cuts the non-convex static sets \mathcal{S}_t are replaced by the convex variant

$$\mathcal{R}_t := \{y_t \geq 0 \mid B_t y_t = b_t, Eg_t \leq H(y_t)\}. \quad (13)$$

As customary in energy management problems, an artificial generating unit with high cost and infinite capacity is considered in each bus. Since nonanticipativity constraints are relaxed, feasibility of the slave problems (9) is therefore ensured (the SUC satisfies the property of relative complete recourse). This is why line 2 of the algorithm generates optimality cuts (10) only.

In line 3, the upper bound calculation takes into account that the solver employed to compute ov^k may not be a global optimization one, and provide only a local solution. The work [LTB11] uses a global optimization solver and sets directly $\text{ub}^k = \text{ov}^k$. We use the NLP solver Ipopt [WB06], so the solution found may correspond to a local minimum. The upper bound definition is changed to keep a record of the smallest value found throughout iterations.

Since the master problems (12) have linear objective and constraints with 0-1 variables and the slave problems (9) are convex, the process that iterates between lines 2 and 4 converges. More precisely, by [Geo72, Theorem 2.4], the process has finite termination because the master

Algorithm 1: Non-convex GBD [LTB11]

Data: starting point x^0 and a tolerance $\varepsilon \geq 0$ for termination.

Set the iteration counter $k = 0$.

1 repeat

2 *Slave solution:* Given x^k , find y^k solving the convex program

$$\begin{cases} \min & f(y) \\ \text{s.t.} & y_t \in \mathcal{R}_t \cap \mathcal{Y}_t \text{ for all } t \\ & Wy \leq h - Tx^k. \end{cases} \quad (9)$$

Let π^k be the optimal multiplier corresponding to the affine constraint above.

Define the optimality cut

$$\mathcal{C}^k(x) := \langle \pi^k, h - Tx \rangle. \quad (10)$$

3 *Upper bound:* Solve the nonlinear programming (NLP) problem

$$\begin{cases} \min & f(y) \\ \text{s.t.} & y_t \in \mathcal{S}_t \cap \mathcal{Y}_t \text{ for all } t \\ & Wy \leq h - Tx^k, \end{cases} \quad (11)$$

and let ov^k be the optimal value. If $k = 0$, set $\text{ub}^0 := \min(f(y^0), \text{ov}^0)$. If $k > 0$, set $\text{ub}^k = \min(f(y^k), \text{ub}^{k-1}, \text{ov}^k)$.

4 *Master problem:* Find (x^{k+1}, α^{k+1}) solution to the 0-1 linear problem

$$\begin{cases} \min & \langle \mathcal{F}, x \rangle + \alpha \\ \text{s.t.} & x_t \in \mathcal{X}_t \text{ for all } t \\ & \alpha \geq \mathcal{C}^\ell(x) \text{ for } \ell = 0, \dots, k, \end{cases} \quad (12)$$

and let lb^{k+1} be the optimal value.

5 *Update:* Set $k = k + 1$.

6 until the gap is sufficiently small: $\text{ub}^k - \text{lb}^k \leq \varepsilon \max(1, |\text{lb}^k|)$ for $k > 0$.

feasible sets \mathcal{X}_t are discrete. We note also that the performance of the non-convex GBD depends on the ability of (globally) solving fast the NLP problem (11) (line 3 in Algorithm 1). In practice, it is common to assign a *time budget* to each block of Algorithm 1. We set a time limit for solving the master problem (12), as suggested by [BCF19].

3.2 Regularization à la level-bundle

Benders decomposition can be slow to converge, particularly for large-scale problems. Already in [GG74] poor performance was observed in some circumstances; see also [MW81]. Essentially, the lower bound of the method tends to stall and oscillate when getting closer to a

solution. This “zig-zagging” phenomenon is well-known in nonsmooth optimization and is related to the cutting-plane approximation done by means of the variable α in (12); see [Bon+06, Example 9.7]. Attempts to tackle such weakness are numerous in the literature and essentially fall into two categories. Acceleration is obtained either by saving on the computational cost per iteration, or by reducing the total number of iterations. Regarding the former, we mention [MD77] and [ZPR00], respectively solving approximately the master and the slaves to accelerate the procedure. The second group of research aims at generating “deeper” cuts, as in [FSZ10], [Cad10], or at stabilizing the oscillations in the master program by means of some regularization, along the lines of bundle methods [Bon+06, Chapter 10]. For two-stage stochastic problems the quadratic regularizations introduced in [Rus86] were explored later on for tackling inexact information provided by the slave problems in [OSS11; OS14]; see also [Fáb+15]. In the context of Benders decomposition for mixed-integer problems the first proposal we found is [ZM14], followed up by [MOZ17]. Our method, Algorithm 2 given in pseudo-code below, falls into this last line of works, and is close to the proximal level bundle method [Kiw95] with the important difference that in that work decision variables are continuous.

The stabilization mechanism devised by bundle methods keeps track along iterations of certain records \hat{x}^k , called *serious* iterates, that provide sufficient descent towards the minimum (cf. the descent test in Algorithm 2, line 4). The master problem (12) is then modified to prevent the next iterate to move “too far away” from the record, depending on a parameter. For instance, a penalized-bundle formulation of (12) defines

$$\begin{cases} \min & \langle \mathcal{F}, x \rangle + \alpha + \frac{1}{2}\mu_k \|x - \hat{x}^k\|^2 \\ \text{s.t.} & x_t \in \mathcal{X}_t \text{ for all } t \\ & \alpha \geq \mathcal{C}^\ell(x) \text{ for } \ell = 0, \dots, k, \end{cases}$$

for a parameter $\mu_k > 0$. In a level-bundle formulation, instead of adding a penalization in the objective function, the master program projects the record onto certain *level set* depending on a parameter denoted by \mathbb{L}^k :

$$\begin{cases} \min & \frac{1}{2} \|x - \hat{x}^k\|^2 \\ \text{s.t.} & x_t \in \mathcal{X}_t \text{ for all } t \\ & \alpha \geq \mathcal{C}^\ell(x) \text{ for } \ell = 0, \dots, k \\ & \langle \mathcal{F}, x \rangle + \alpha \leq \mathbb{L}^k. \end{cases}$$

If the parameter \mathbb{L}^k is too low (for instance smaller than the desired optimal value), the problem above can be infeasible. In this case, the level-bundle method increases the parameter and solves a new master problem. To converge, \mathbb{L}^k is adjusted using lower and upper bounds (denoted f_{lo}^k and f_{up}^k below) that “sandwich” the optimal value, as long as iterates remain in a compact set (compactness is automatic in our case, because each \mathcal{X}_t is contained in a hypercube).

An important feature of bundle methods is that, unlike the Benders’ master program (12), they generate a monotone subsequence of iterates (the “serious steps” in line 4 below). The corresponding lower bounds are superior to the ones obtained with Algorithm 1.

Our stabilized master problem (14) uses so-called proximal level variant [Kiw95], that allows for compressing the bundle information (and, therefore, can reduce the number of cuts while maintaining the convergence properties of the method).

At first sight, when dealing with mixed-0-1 decision variables, inserting a proximal, quadratic, stabilization is not practical, because the master program becomes a quadratic programming problem with mixed 0-1 variables. For this reason, [Oli16] considers only polyhedral norms. In our setting, however, the fact that the master program has only binary variables enables regularizations in the Euclidean norm, simply because quadratic terms involving only 0-1 variables are in fact linear:

$$\text{given } \hat{x}^k \in \{0, 1\} \text{ a parameter, } \frac{1}{2}(x - \hat{x}^k)^2 = \frac{1}{2}(x + \hat{x}^k) - x\hat{x}^k \text{ for all } x \in \{0, 1\}.$$

As a result, in line 13 of Algorithm 2 at the k th iteration the objective function in (14) coincides with $\frac{1}{2}\|x - \hat{x}^k\|^2$, making the master program a projection of the reference point \hat{x}^k onto the level set, as usual in level bundle methods.

Algorithm 2: Non-convex GBD with Proximal Level Bundle Stabilization

Data: starting point x^0 , parameters $m, \kappa \in (0, 1)$, and a tolerance $\varepsilon \geq 0$.

Set the iteration counter $k = 0$, and $f_{\text{up}}^0 = +\infty$, $\Delta^0 := 0$.

1 repeat

2 *Slave solution:* Given x^k , find y^k solving the convex program (9) and define the k th optimality cut (10). Let v^k denote the optimal value.

3 *Upper bound:* Compute ov^k the optimal value of (11). If $k = 0$, set $\text{ub}^0 := \min(v^0, \text{ov}^0)$. If $k > 0$, set $\text{ub}^k = \min(v^k, \text{ub}^{k-1}, \text{ov}^k)$.

4 *Level-bundle descent test*

Compute f_{lo}^k the optimal value of (12), and the bundle gap $\Delta^k := f_{\text{up}}^k - f_{\text{lo}}^k$.

If $\langle \mathcal{F}, x^k \rangle + v^k \leq f_{\text{up}}^k - m\Delta^k$, then $\begin{cases} \hat{x}^k = x^k \\ f_{\text{up}}^k = \min(f_{\text{up}}^k, \langle \mathcal{F}, x^k \rangle + v^k) \end{cases}$ [*serious step*]

Otherwise, set $\hat{x}^k = \hat{x}^{k-1}$ and $f_{\text{up}}^k = f_{\text{up}}^{k-1}$ [*null step*].

5 *Master problem:* Given $\hat{x}^k \in \{0, 1\}^{Nx}$, find (x^{k+1}, α^{k+1}) solving the 0-1 linear problem

$$\begin{cases} \min & \sum_{n=1}^{Nx} \left(\frac{1}{2}(x_n + \hat{x}_n^k) - x_n \hat{x}_n^k \right) \\ \text{s.t.} & x_t \in \mathcal{X}_t \text{ for all } t \\ & \alpha \geq \mathcal{C}^\ell(x) \text{ for } \ell = 0, 1, \dots, k \\ & \langle \mathcal{F}, x \rangle + \alpha \leq \kappa f_{\text{lo}}^k + (1 - \kappa) f_{\text{up}}^k. \end{cases} \quad (14)$$

Feasibility check: If (14) is feasible, let $\text{lb}^{k+1} = f_{\text{up}}^{k+1}$. Otherwise, if problem (14) is infeasible, increase $f_{\text{lo}}^k = \kappa f_{\text{lo}}^k + (1 - \kappa) f_{\text{up}}^k$ and loop to line 5.

6 *Update:* Set $k = k + 1$.

7 until the gap is sufficiently small: $\text{ub}^k - \text{lb}^k \leq \varepsilon \max(1, |\text{lb}^k|)$ for $k > 0$.

Although not defined explicitly, in Algorithm 2 the level parameter is $\mathbb{L}^k := \kappa f_{\text{lo}}^k + (1 - \kappa) f_{\text{up}}^k$. The extra calculation to compute f_{lo}^k in line 4 can be skipped, we refer [OS14] for details. As with Algorithm 1, we impose a time budget for solving the master problem (14) at each iteration.

3.3 The full SUC solver

Table 1 contains some notation useful to explain how to incorporate the stochastic ingredients in Algorithm 2 when there is a finite number of strategic scenarios (process ω) and an operational fan (process ξ), defined at different time scales.

Table 1: Uncertainty discretization: some notation.

Data process	One realization	Probability	Time set	Scenario set	Links
Strategic	ω_t^i	p_t^i	\mathbb{T}^x	\mathbb{I}	$i_{\nu(t,j)}$
Operational	ξ_t^j	\tilde{p}_t^j	\mathbb{T}^y	\mathbb{J}	$j_{\nu(t,i)}$

The connection between nodes in the two sets is given by means of a linking mapping ν , which depends on t and on the considered scenario. Namely, given an operational realization ξ_t^j , its corresponding commitment realization is $\omega_t^{i_{\nu(t,j)}}$ and similarly in the reverse direction, noting that the mapping may be empty, a singleton or a set. To illustrate these concepts, consider the example in Figure 3. The time and scenario index sets therein are

$$\mathbb{T}^x = \{1, 3, 4\}, \mathbb{T}^y = \{1, 2, 3, 4\} \quad \text{and} \quad \mathbb{I} = \{1, 2, 3, 4\}, \mathbb{J} = \{1, 2, \dots, 8\}.$$

The first strategic scenario $(\omega_1^1, \omega_3^1, \omega_4^1)$ in the figure has scenario index $i = 1$ and the links are

$$\begin{aligned} \text{for } t = 1 : \quad & i_{\nu(t,j)} = 1 \quad \text{for } j = 1, \dots, 8 \quad \text{and} \quad j_{\nu(t,1)} \in \{1, \dots, 8\} \\ \text{for } t = 2 : \quad & i_{\nu(t,j)} = 1 \quad \text{for } j = 1, \dots, 4 \quad \text{and} \quad j_{\nu(t,1)} = \emptyset \\ \text{for } t = 3, 4 : \quad & i_{\nu(t,j)} = 1 \quad \text{for } j = 1, \dots, 4 \quad \text{and} \quad j_{\nu(t,1)} \in \{1, \dots, 4\}. \end{aligned}$$

With this notation, the commitment associated with each operational decision is

$$x_{t_x}^{i_{\nu(t_y,j)}} \leftrightarrow y_{t_y}^j \quad \text{for all } t_x \in \mathbb{T}^x, t_y \in \mathbb{T}^y, \text{ and } j \in \mathbb{J},$$

and, to take into account only operational decisions linked with each commitment, we define

$$\mathbf{p}_t^{i,j} := \begin{cases} p_t^i \tilde{p}_t^j & \text{if } j \in j_{\nu(t,i)} \\ 0 & \text{otherwise.} \end{cases}$$

The SUC problem to be solved has the form

$$\left\{ \begin{array}{ll} \min & \sum_{i \in \mathbb{I}} \sum_{t \in \mathbb{T}^x} p_t^i \langle \mathcal{F}_t, x_t^i \rangle + \sum_{j \in \mathbb{J}} \sum_{t \in \mathbb{T}^y} \mathbf{p}_t^{ij} f_t(y_t^j) \\ \text{s.t.} & x_t^i \in \mathcal{X}_t(\omega_{[t]}^i) & \text{for all } t \in \mathbb{T}^x, \text{ and } i \in \mathbb{I} \\ & y_t^j \in \mathcal{S}_t(\xi_t^j) \cap \mathcal{Y}_t(\xi_t^j) & \text{for all } t \in \mathbb{T}^y, \text{ and } j \in \mathbb{J} \\ & Tx^i + Wy^j \leq h \text{ where } i \in \{i_{\nu(t_y,j)} \mid t_x \in \mathbb{T}^x, t_y \in \mathbb{T}^y\} & \text{for all } j \in \mathbb{J}. \end{array} \right.$$

The full SUC solver presented as Algorithm 4 in the appendix modifies Algorithm 2 to deal with a larger master problem, with variables x_t^i for $t \in \mathbb{T}^x$ and $i \in \mathbb{I}$. The variable α in (14) now represents a cutting-plane approximation of an expected value function, obtained by averaging cuts (10) while looping over the suitable portion of the operational fan, to solve the corresponding slave problems. Optimal values and bounds are also taken in average. See Appendix A for details.

4 Implementational considerations

Algorithm 2 performance depends on how its main blocks are implemented. We review some key issues, relative how to define the convexified set \mathcal{R}_t from (13), so that (8) holds numerically, and to how to build a good initial point when (globally) solving the the NLP problem (11) (line 3 in Algorithm 1 and line 5 in Algorithm 4).

4.1 Approximating the non-concave hydro-production function

As mentioned, when (8) holds, that is when H is a concave function that overestimates the hydro-production function hp over the set \mathbb{Z} , problem (9) is a convex relaxation of the the NLP problem (11).

The convex relaxation is defined for each unit of each hydro-power plant, whose HPF depends on the turbined outflow q of the unit, spillage s , volume v of the reservoir, and the sum Q of the turbined outflow of all units of the hydro-power plant. Given lower and upper bounds l_q, l_s, l_v and u_q, u_s, u_v , by the nature of these variables, it suffices to satisfy (8) over the set

$$\mathbb{Z} := \left\{ z := (q, s, v, Q)^\top \in \mathbb{R}^4 \mid l_q \leq q \leq u_q, l_s \leq s \leq u_s, l_v \leq v \leq u_v, q \leq Q \leq u_Q \right\},$$

where $u_Q := \sum_q u_q$. We build a concave quadratic function H that satisfies (8) only over points in a given finite set $Z \subset \mathbb{Z}$. The approximation has the expression

$$H(z) := \langle z, M^* z \rangle + \langle m^*, z \rangle + \mu^*,$$

where the matrix, vector and number (M^*, m^*, μ^*) solve the convex semidefinite problem

$$\begin{cases} \min & \sum_{z_i \in Z} \left(\langle z_i, M z_i \rangle + \langle m, z_i \rangle + \mu \right) \\ \text{s.t.} & M \in \mathbb{R}^{4 \times 4}, m \in \mathbb{R}^4, \mu \in \mathbb{R}, \text{ with } M \preceq 0, \\ & \text{hp}(z_i) \leq \langle z_i, M z_i \rangle + \langle m, z_i \rangle + \mu \text{ for all } z_i \in Z. \end{cases} \quad (15)$$

The choice of the objective function is meant to make the approximation tight. In our experiments, the set Z has 160,000 points and we used the package SDPT3 version 4.0 [TTT03] for solving problem (15).

4.2 Initial point for the non-convex problem

For ensuring good performance, it is important to provide a good starting point when solving the non-convex problem (11) providing upper bounds. [In a manner similar to the construction of the concave quadratic function \$H\$ in Section 4.1, we build a concave quadratic function \$H^u\$ that underestimates the hydro-production function \$\text{hp}\$ over the same set \$\mathbb{Z}\$ by letting](#)

$$H^u(z) := \langle z, M^{u*} z \rangle + \langle m^{u*}, z \rangle + \mu^{u*},$$

where the matrix, vector and number $(M^{u*}, m^{u*}, \mu^{u*})$ solve a convex semidefinite problem like (15), with the inequality constraint reversed, that is

$$\text{hp}(z_i) \geq \langle z_i, M z_i \rangle + \langle m, z_i \rangle + \mu \text{ for all } z_i \in Z.$$

We then define the set $\mathcal{U}_t := \{y_t \geq 0 \mid B_t y_t = b_t, E g_t \leq H^u(y_t)\}$ and consider the problem

$$\begin{cases} \min & f(y) \\ \text{s.t.} & y_t \in \mathcal{U}_t \cap \mathcal{Y}_t \text{ for all } t \\ & W y \leq h - T x^k, \end{cases} \quad (16)$$

which is, in some sense, a convex approximation of problem (11). The solution y^k of problem (16) is employed to construct a good feasible initial point for (globally) solving the NLP problem (11) (line 3 in Algorithm 1 and line 5 in Algorithm 4). The procedure is given in Algorithm 3 below. Therein, the thermal and hydro-generation are denoted by g^T and g^H , the turbined outflow by q , the spillage by sp , the reservoir volume by v , the voltage angles by θ . The generation of the artificial thermal unit with infinite capacity is g^∞ .

Algorithm 3: Starting point for the non-convex minimization problem

Data: $\alpha \in (0, 1)$ and y^k solving (16).
Initialize g^T, q, sp, v, θ , and g^∞ with the corresponding components in y^k .
Set $fix_water_balance \leftarrow \text{false}$.

- 1 **foreach** hydro-plant h , unit u , and time t **do**
 - Compute the value g_{thu}^H of the non-convex HPF hp.
 - if** $g_{thu}^H > \Gamma_{thu}$ **then**
 - Reduce q_{thu} by letting $q_{thu} \leftarrow \alpha q_{thu}$. Let $fix_water_balance \leftarrow \text{true}$. **Go to** 1
- 2 **end**
- 3 **end**
- if** $fix_water_balance = \text{true}$ **then**
 - 4 **foreach** hydro-plant h and time t **do**
 - Compute the values of v_{th} and sp_{th} so that the water balance constraint is satisfied. Let $fix_water_balance \leftarrow \text{false}$. **Go to** 1
 - 5 **end**
- 6 **end**
- 7 **foreach** bus b and time t **do**
 - Compute the value of g_{tb}^∞ so that the power balance constraint is satisfied.
- 8 **end**

Inside the loop defined in line 4 of Algorithm 3, we recompute the values of v_{th} and sp_{th} since the associated water balance constraint cannot be satisfied if the outflow q_{thu} of some unit u of hydro-plant h has been reduced within the loop defined in line 1. In order to satisfy the water balance constraint, the amount of water that is no longer flowing through the units is put back into the reservoir. If this amount exceeds the maximum capacity of the reservoir, the excess of water is added to the spillage sp_{th} .

4.3 Measuring proximity between scenarios: the sustainable pseudo-distance

The output of the SUC solution using Algorithm 2 is a policy with optimal commitments and operational decisions, for the considered strategic scenario tree and operational fan, with

components linked by the mapping ν in Table 1:

$$\bar{x}_{t_x}^i \text{ for } i \in \mathbb{I}, t_x \in \mathbb{T}^x \quad \text{and} \quad \bar{y}_{t_y}^j \text{ for } j \in \mathbb{J}, t_y \in \mathbb{T}^y.$$

In order to assess the quality of the obtained solution, we put in place a simulation phase that mimics the system operation for a large fan of out-of-sample operational scenarios, say

$$O^y := \left\{ \xi_{[\mathbb{T}^y]}^o \mid o = 1, \dots, 10,000 \right\}.$$

Given an out-of-sample scenario in O^y with index o , suppose we are given the index $jo \in \mathbb{J}$ of the *closest* in-sample operational scenario, $\xi_{[\mathbb{T}^y]}^{jo}$. Then the NLP problem

$$\left\{ \begin{array}{ll} \min & \sum_{t \in \mathbb{T}^y} f_t(y_t) \\ \text{s.t.} & y_t \in \mathcal{S}_t(\xi_t^o) \cap \mathcal{Y}_t(\xi_t^o) \\ & T\bar{z}^{jo} + Wy \leq h \\ & \bar{z}^{jo} := \left(\bar{x}_{t_x}^{i\nu(t_y, o)} \mid t_x \in \mathbb{T}^x, t_y \in \mathbb{T}^y \right) \end{array} \right. \quad \text{for all } t \in \mathbb{T}^y$$

simulates the operation of the system under the considered scenario realization.

To define the closest in-sample-scenario we modify the pseudo-distance introduced in [Oli+10], successfully applied in mid-term power planning problems, to take the most advantage of wind power, thus justifying the naming “sustainable”.

Suppose scenarios are N -dimensional and let each component be denoted by $\xi_{[\mathbb{T}^y]}^j(n)$ for $n = 1, \dots, N$. Let $\psi_t(n)$ denote the n -th component of the uncertain right-hand side terms a_t and b_t in (1), respectively corresponding to the inflows and bus loads (the latter vary with the uncertain wind).

Given a reference scenario, $\xi_{[\mathbb{T}^y]}^o$, to find the scenario that is closest the notion of distance and proximity needs to be precised. Each scenario has \mathbb{T}^y components that are N -dimensional. The well-known ℓ_∞ and ℓ_1 -distances between those two scenarios are, respectively,

$$\max_{n \leq N} \max_{t \in \mathbb{T}^y} \left| \xi_t^j(n) - \xi_t^o(n) \right| \quad \text{and} \quad \sum_{n \leq N} \sum_{t=1}^{\mathbb{T}^y} \left| \xi_t^j(n) - \xi_t^o(n) \right|.$$

An in-between distance, ℓ_∞ on the n -components and ℓ_1 on the t -components would be

$$\max_{n \leq N} \sum_{t=1}^{\mathbb{T}^y} \left| \xi_t^j(n) - \xi_t^o(n) \right|,$$

We use the proximity measure above, scaled, as follows:

$$\check{d}(\xi_{[\mathbb{T}^y]}^j, \xi_{[\mathbb{T}^y]}^o) := \max_{n \leq N} \sum_{t=1}^{\mathbb{T}^y} d_t^n \left| \xi_t^j(n) - \xi_t^o(n) \right|. \quad (17)$$

In order to better capture extreme scenarios without losing the proximity to the mean, we employ the scaling factor

$$d_t^n := \sqrt{\psi_t(n)} \max \left\{ 1, \psi_t(n)(\xi_t^j(n))^2, \psi_t(n)(\xi_t^o(n))^2 \right\}.$$

We refer to [Oli+10], where a similar notion was successfully employed for selecting inflow scenarios in the Brazilian power system. The closest scenario minimizes \check{d} over all $j \in \mathbb{J}$.

Because of the use of an absolute value, the proximity notion above is indifferent to the *sign* of the term $\xi_t^j(n) - \xi_t^o(n)$. This may result in choosing as closest scenario $\xi_t^{j^o}$ one having more wind power than the considered out-of-sample scenario, with index o . A system configuration with more wind power is not cost-efficient if there is not enough wind (as with $\xi_{[\mathbb{T}^y]}^o$), and can even result in load shedding. For this reason, we redefine the pseudo-distance

$$D_t^n(\xi_{[\mathbb{T}^y]}^j, \xi_{[\mathbb{T}^y]}^o) := \sqrt{\psi_t(n)} \chi_t(n) (\xi_t^j(n) - \xi_t^o(n)) \max \left\{ 1, \psi_t(n) (\xi_t^j(n))^2, \psi_t(n) (\xi_t^o(n))^2 \right\},$$

with $\chi_t(n) = 1$ if n corresponds to a component of demand on a bus, and is set to -1 otherwise. The closest scenario is chosen as follows. If the optimal value of the problem below is non-negative,

$$\begin{cases} \min & \sum_{t=1}^{\mathbb{T}^y} D_t^n(\xi_{[\mathbb{T}^y]}^j, \xi_{[\mathbb{T}^y]}^o) \\ \text{s.t.} & j \in \mathbb{J}, n = 1, \dots, N, \end{cases}$$

then j^o is the index of the minimizing scenario. Otherwise, j^o is the index of the scenario solving the problem below

$$\begin{cases} \min & \max_{n \leq N} \sum_{t=1}^{\mathbb{T}^y} D_t^n(\xi_{[\mathbb{T}^y]}^j, \xi_{[\mathbb{T}^y]}^o) \\ \text{s.t.} & j \in \mathbb{J} \text{ satisfies } D_t^n D_t^n(\xi_{[\mathbb{T}^y]}^j, \xi_{[\mathbb{T}^y]}^o) \leq 0. \end{cases}$$

5 Numerical results

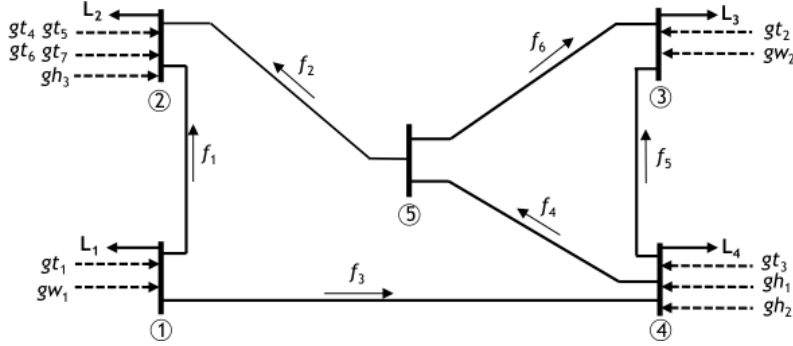
The numerical assessment was done with a hydro-thermal configuration based on a reduced variant of the southern Brazilian system, described below. The results are organized as follows: first, we present several (convex) instances comparing the Generalized Benders Decomposition with the Proximal Level Bundle variant, in which only the convex strategic subproblems are considered. Then we compare the performance of the proximity measures on an out-of-sample simulation for the non-convex commitment obtained when running Algorithm 4. Finally, we present different indicators that confirm the superiority of the non-convex model over the convex one, both in-sample and out-of-sample-wise.

5.1 The hydro-thermal system

There are 21 units (12 hydro-units (gh_i) located in three reservoirs, 7 thermal units (gt_i), and 2 wind farms (gw_i)). The transmission system has 6 lines (f_i) and 5 buses (\textcircled{i}) and connects the generating units to 4 load demands (L_i). Figure 4 depicts the system, where the hydro gh_1 is upstream to gh_2 and has one-hour water travel time. The total installed capacity of the hydro-generation is 4270 MW and the thermal generation is 1447 MW. We consider a 24-hour planning horizon, where the minimum and maximum values of the total demand in the system is 3411 MW and 3515 MW, respectively. The inflows and the wind generation are considered

the random variables, both modeled as lag-one autoregressive models with different parameters obtained from historical data. More details about the system can be found in Appendix B.

Figure 4: Schematic diagram of the hydro-thermal system.



The HPF is defined as in [FS13]. The power generation (hp) of a single hydro-unit that belongs to a specific hydro-plant and period is given by $\text{hp} = 9.81 \cdot 10^{-3} \eta h q$ where η , h , and q are the efficiency, net head, and turbined outflow of the unit, respectively. However, only q is a decision variable in a hydro-plant. The efficiency is a function of h and q ; in turn, the net head depends on the volume of the reservoir (v), turbined outflow (q), and spillage (s) of the plant. Thus, the control variables in a hydro-plant are q and s , and the volume is a state variable. Thus, $h := h(q, s, v)$, $\eta := \eta(q, s, v)$, and the following expression must be included in (1) to represent the HPF: $h = \sum_{i=0}^4 D_i v^i - \sum_{i=0}^4 E_i (Q + s)^i - G q^2$ and $\eta = F_0 + F_1 q + F_2 h + F_3 q h + F_4 q^2 + F_5 h^2$, where Q is the total discharge through all turbines of the hydro-plant, and D_0, \dots, D_4 , E_0, \dots, E_4 , F_0, \dots, F_5 and G are peculiar constants of each hydro-plant and generating unit. As a result, the HPF of a single unit is a high-order non-convex function. The main data related to the HPF of the units of the system can be found in Table 2.

Plant	G	D_0	D_1	D_2	D_3	D_4
1	5.603×10^{-6}	431.694	0.0146766	0	0	0
2	1.9×10^{-5}	331.649	0.0075202	0	0	0
3	1.107×10^{-5}	681.949	0.0110377	0	0	0

Plant	E_0	E_1	E_2	E_3	E_4
1	371.936	0.00151449	0	0	0
2	261	0.00301	-5.64×10^{-7}	6.79×10^{-11}	-3.03×10^{-15}
3	601.886	0.00175726	0	0	0

Plant	F_0	F_1	F_2	F_3	F_4	F_5
1	0.3587	0.0024	0.0036	8.13×10^{-6}	-4.91×10^{-6}	-3.12×10^{-5}
2	0.2519	0.0029	0.0065	1.86×10^{-5}	-9.19×10^{-6}	-5.65×10^5
3	0.3587	0.003	0.0026	7.37×10^{-6}	-7.77×10^{-6}	-1.62×10^{-5}

Table 2: Values of the constants for each hydro-plant.

Units in a hydro-plant are identical, but differ among different hydro-plants.

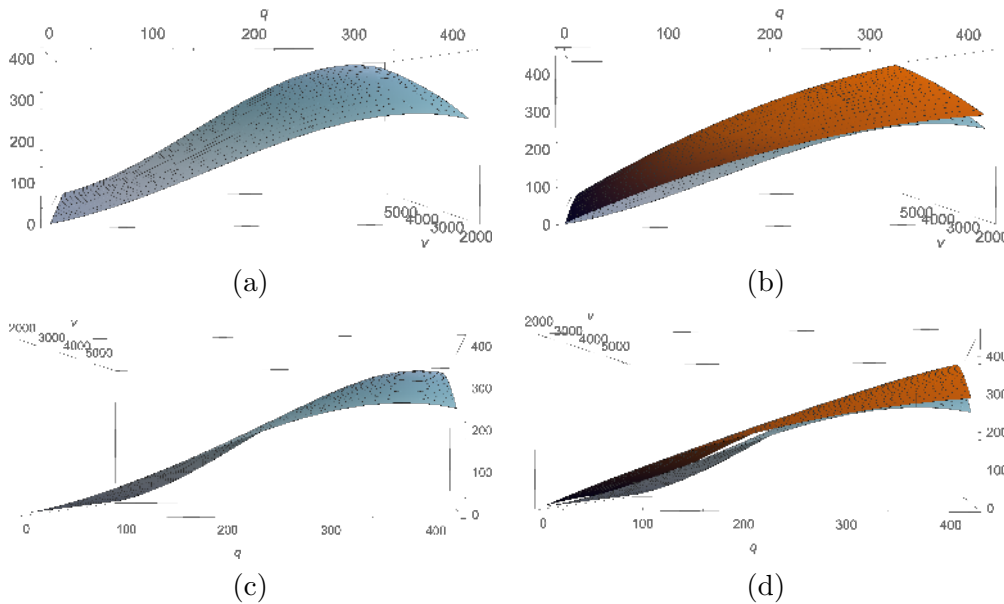
The quadratic convex approximations for the HPF in Section 4.1 are built considering for each hydro-plant a set Z with 160,000 points. The quality of the approximations is summarized by the results in Table 3, measuring the distance between the non-convex HPF and the convex approximations, over one million points uniformly distributed over the domain of the function. As the convex approximation is not an exact overestimator of the non-convex HPF, it is lower than the non-convex HPF on some points. Columns 2 and 3 of Table 3 show, respectively, the average and maximum violations (distance between the values of the functions on points in which the convex approximation is lower than the HPF) for each approximation. Columns 4 and 5 show, respectively, the average and maximum distances of the values of the functions on points in which the convex approximation indeed overestimates the HPF.

Plant	Average violation	Maximum violation	Average distance	Maximum distance
1	1.4×10^{-7}	0.1975	37.1094	65.9753
2	3.7×10^{-8}	0.1989	16.9369	34.2568
3	1.4×10^{-7}	0.1911	28.6733	54.4695

Table 3: Violations and distances (in MW) between the non-convex HPF and its convex approximations over one million points.

Figure 5 illustrates the non-convex HPF and the convex approximation for one unit of hydro-plant 2, where $q = Q \in [l_q, u_q]$, $v \in [l_v, u_v]$ (only one operating unit) and $s = 0$ (there is no spillage). Views for the non-convex (respectively convex) HPF approximations are shown in Figures 5(a) and 5(c) (respectively, Figures 5(b) and 5(d)).

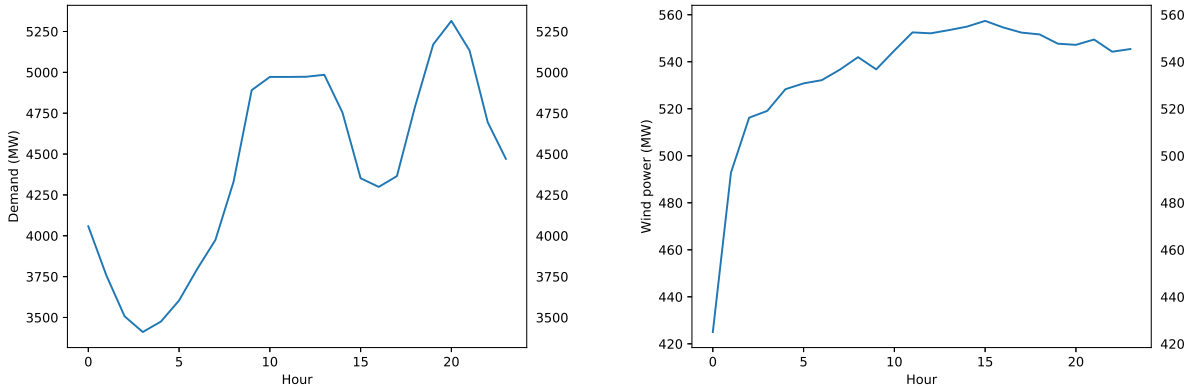
Figure 5: Non-convex HPF function (left) and quadratic convex approximation (right).



The computational results were performed on a 3.4GHz Intel Core i7-3770 machine with 16GB RAM memory and Ubuntu 16.04 (GNU/Linux 4.4.0-59-generic x86_64) operating system. Algorithms 1 and 4 are coded in C++ and compiled with GCC 5.4.0, with the `-O3` option enabled. All MILPs were solved using CPLEX [IBM11] version 12.6.3 on a single thread and adjusted with 10^{-4} optimality gap tolerance. The Benders decomposition method stops when the relative optimality gap falls below 5×10^{-4} . For the non-convex subproblems, we used Ipopt [WB06] version 3.12.6 with convergence tolerance set to 10^{-4} . In all instances, we consider a MILP master problem with a 63-node scenario-tree structure associated with the strategic decisions. In turn, there are 64 continuous subproblems related to the operational decisions.

Full details on the system can be found in Appendix B. Figure 6 illustrates the system demand and the average wind power. Notice in particular that demand peaks at hour 20.

Figure 6: Demand (left) and average wind power (right).



5.2 Bundle method performance

We start by benchmarking the performance of the stochastic version of Algorithm 1 and Algorithm 4 on the convex formulation of the problem. This means that at each iteration of Algorithms 1 and 4, we solve problem (9) but not problem (11). We considered 100 randomly generated scenario trees for this experiment.

The time budget, setting a time limit of 10 seconds to solve the master problem at each iteration, appears to be fundamental for Algorithm 4 to perform efficiently. We compare the algorithms in two different versions, one considering a time limit for solving the master problem ((12) or (18)), and the other without time limit. Algorithms with a time limit for solving the master problem are indicated by the superscript ^{TL}.

Algorithm 1 and Algorithm 4^{TL} were able to solve all instances, requiring at most 31 iterations; while Algorithm 1^{TL} could not solve 7 instances within the maximum number of iterations, set to 100 for all solvers. If the time limit to solve the master problem is reached, there is no guarantee that the returned solution is optimal and, therefore, it cannot be used to improve the

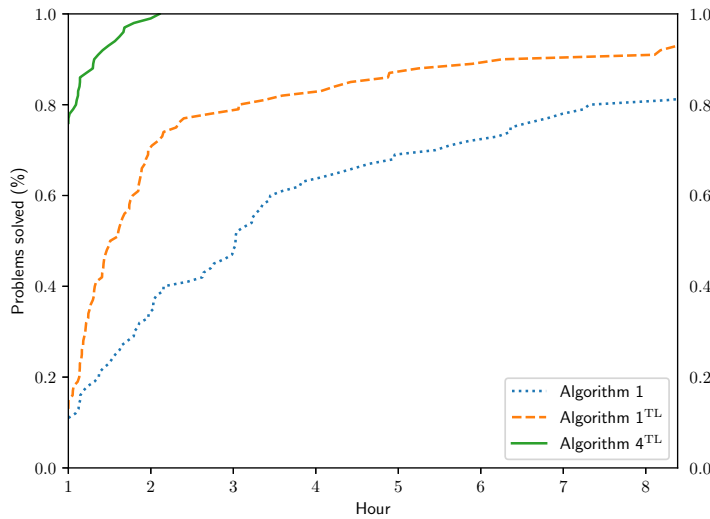
	Average time (s)	Minimum time (s)	Maximum time (s)	Minimum # iterations	Maximum # iterations
Algorithm 1	1515	101	11807	12	31
Algorithm 1 ^{TL}	487	121	2016	12	100
Algorithm 4 ^{TL}	206	120	498	11	29

Table 4: Performance of the algorithms when solving the 100 considered instances.

lower bound. This may require a higher number of iterations for the method to close the gap, which is one of the reasons why Algorithm 1^{TL} could not solve all instances within 100 iterations (this is also the reason for including in the table results for Algorithm 1 without any time budget). Table 4 shows the average, minimum, and maximum time (in seconds) for solving an instance of the problem, as well as the minimum and maximum number of iterations required. Notice that Algorithm 4^{TL} has the lowest average time for solving an instance. On average, Algorithm 4^{TL} is 7.35 times faster than Algorithm 1 and 2.36 times faster than Algorithm 1^{TL}. Algorithm 4^{TL} was faster than Algorithm 1 and Algorithm 1^{TL} for 88 and 80 instances, respectively. Moreover, the stabilized version provided an average reduction of the running time of 51% and a maximum reduction of 98% in comparison with Algorithm 1. In comparison with Algorithm 1^{TL}, those figures are 31% and 92%, respectively.

The performance profile in Figure 7, illustrating graphically the behaviour of the three solvers, confirms the superiority of the bundle-like Algorithm 4^{TL}. Incidentally, the difference between the two bottom lines, corresponding to Algorithm 1 with and without a time limit, confirm the interest of using time budgets in the master solution.

Figure 7: Performance profile for Algorithm 1, Algorithm 1^{TL}, and Algorithm 4^{TL}.



5.3 Output of the convex and non-convex optimization problems

Consider Algorithm 4. Let k_1 be the iteration number in which problem (9) attains its lowest value and k_2 be the iteration number in which problem (11) attains its lowest value. When $k_1 = k_2$, there is no reason to solve problem (11), thus making the solution process a lot faster. In what follows, we compare the commitment associated with the best solution of the convex subproblem (9), x^{k_1} , with the commitment associated with the best solution of the non-convex subproblem (11), x^{k_2} . We call the former the convex commitment and the latter the non-convex commitment. We define the cost of a commitment as the sum of the optimal value of problem (11) associated with that commitment and the cost of starting up and shutting down units in this commitment. We have considered 100 instances of the problem and solved each of them with Algorithm 4^{TL}. We set a time limit of 10 seconds to solve the master problem (14) at each iteration, as this version provided better results as shown in Section 5.2. In mean, each run was completed in 2h03m.

Among the 100 scenario-tree instances, the convex and non-convex commitments are different in 67 instances. Considering only those instances whose convex and non-convex commitments differ, the cost of the non-convex commitment is always lower than that of the convex commitment. On average, the cost of the non-convex commitment is 0.18% lower than that incurred by the convex commitment, having the maximum cost reduction of 0.60% for one of the instances. Barring the future cost of water, considering only the immediate cost (start-up, shut-down, and unit variable costs), then the non-convex commitment is 2.10% lower on average and, for one of the instances, it is 8.84% lower. This gives an indication that it is worth solving the non-convex subproblems if the extra computational effort required for this task can be afforded. This observation is supported by the out-of-sample simulation presented below.

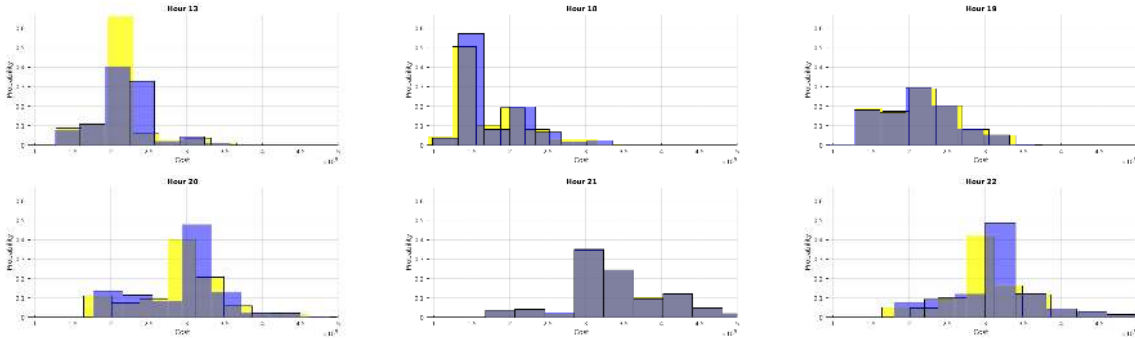
5.4 Out-of-Sample simulation

To assess the commitment decisions in scenarios that are different from the ones employed for solving the SUC problem, we employ the two measures introduced in Section 4.3.

For each out-of-sample scenario, the closest in-sample strategic scenario is found by considering the pseudo-distance (17) and the sustainable measure defined in Section 4.3. The corresponding optimal commitment is then fixed and the non-convex NLP problem (11) (line 3 in Algorithm 1 and line 5 in Algorithm 4) is (globally) solved, for 1000 out-of-sample scenarios. The process was repeated for 100 randomly generated scenario trees, hence solving up to optimality 100 SUC problems with time limit of 10 seconds for the master program solution, as in Section 5.3. Each scenario tree was used in a convex and non-convex formulations of the SUC problem, solved with Algorithm 4^{TL}. In both cases, the output corresponds to the commitment found at the iteration with the lowest cost. As a result, for the non-convex and convex models, and for both the pseudo and sustainable measures of proximity, there is a total of $1000 \times 100 = 100,000$ simulations.

In order to determine if there is a clear winner among the selection strategies, we analyze the simulation thermal costs on the non-convex model for different hours of the day. Figure 8 shows histograms for times in {13, 18, 19, 20, 21, 22}h, in blue (dark color) for the pseudo-distance, and in yellow (light color) for the sustainable proximity measure.

Figure 8: Cost distribution for pseudo (blue) and sustainable (yellow) measures.

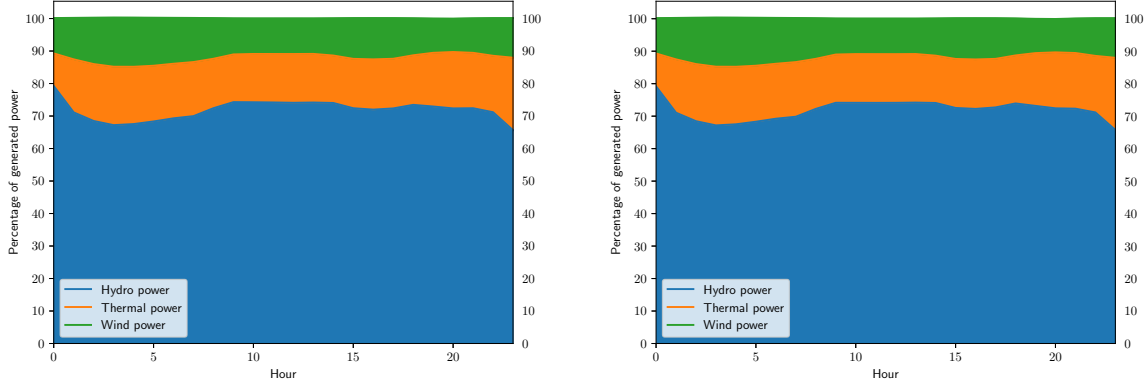


The histogram ordinate displays the probability of occurrence of the cost values given in the abscissa. In particular, the middle bottom graph, corresponding to 21h, is shifted more to the right, when compared to the top middle graph, corresponding to 18h. This reflects the fact that operational costs are higher near peak times (21h). Note, in addition, that at 21h there is practically no blue or yellow in the graph, because both distributions almost coincide. The remaining five graphs exhibit some yellow or blue bars whose meaning is the following. At 13h, the top left graph, the yellow bar indicates that with probability larger than 0.6 the sustainable simulation resulted in an operational cost of about 2×10^5 . By contrast, the pseudo simulation probability of having the same cost is 0.4. The situation is inverted for the next bar, corresponding to the higher cost 2.5×10^5 : the pseudo simulation probability is larger than 0.3, while with the sustainable measure the probability is smaller than 0.1. For the hour 13, simulating with the pseudo distance is likely to result in higher costs. A similar analysis can be done on the other hours, as in each histogram blue bars are higher (more likely) than the yellow ones, and generally shifted towards the right (the region with higher costs). As the probability distributions for the hours that are not displayed in Figure 8 were almost identical with both approaches, the sustainable proximity measure appears as a preferable criterion to determine the closest scenario in simulations.

Having determined the best simulation technique to be employed, we now compare several performance indicators of the convex and non-convex commitments using the sustainable proximity measure. Figure 9 plots the mix of power obtained when using the non-convex and convex formulations. The values are displayed as a percentage of the total generation, taking the mean of over the 100,000 (sustainable) simulations. At first sight, both approaches yield a similar power mix. However, when inspecting closely the output, some important differences arise. The most significant ones refer to the amount of load shedded and the available thermal power near peak times, illustrated in Figure 10.

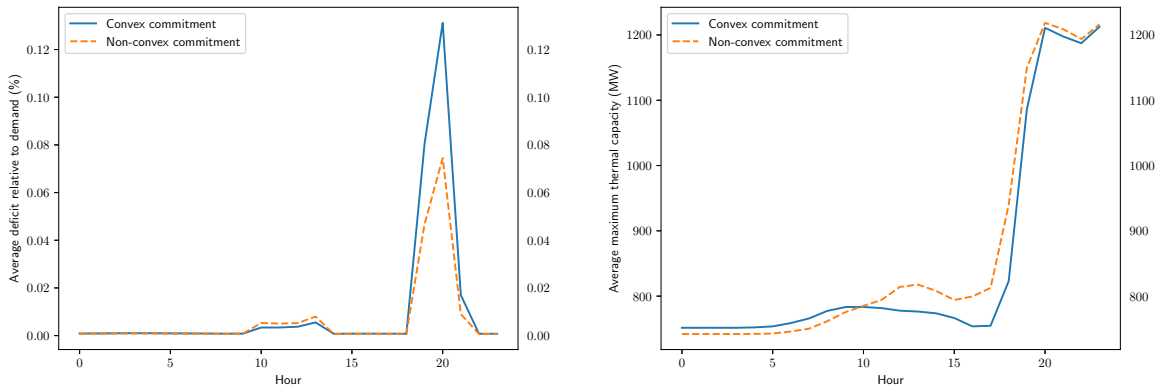
The left graph in Figure 10, showing the average amount of unsatisfied load as a percentage of the demand, exhibits a jump near the hour 20. The deficit of the convex model almost doubles the non-convex one. This phenomenon is explained by the right graph, displaying the maximum thermal capacity that is available with each model: with the convex approach the system has less thermal power available than the non-convex one. With the optimistic convex approximation

Figure 9: Non-convex (left) and convex (right) average power mix.



of the HPF, turbined outflows appear as if providing more energy than what they actually do at simulation (employing the non-convex HPF). Because of the ramp constraints, the convex model does not switch on enough thermal plants in time and incurs in a deficit near the peak.

Figure 10: Non-convex and convex average deficit (left) and available thermal power (right).



The proof-of-concept numerical experience in this section shows that the non-convex SUC model provides results that are better than those of the convex model, in a reasonable computational time (2h in average). Larger systems and larger trees require computational enhancements such as parallelization, warm starts and cut selection procedures. Those specialized techniques are beyond the scope of this work, and are left for future work.

6 Final considerations

We proposed a solution strategy for the stochastic non-convex hydro-thermal unit-commitment based on multi-horizon trees.

By combining a tree on the strategic decision level with a fan of independent scenarios in the operational level, we were able to consider uncertainty in both strategic and operational decision levels. Representing uncertainty in the strategic level is particularly suited for flexible thermal units that can change its on/off-status over the day, to respond fast to variations in the wind generation. To deal with thermal units with slow dynamics, like coal-fired plants, the generation ramps should be chosen so that changes in the on/off status occur along longer time periods (this feature reduces the number of 0-1 variables in the problem).

For solving the problem, we introduced a bundle-like regularization method that stabilizes the Generalized Benders decomposition. Results showed that the stabilized version is much faster than the original Generalized Benders decomposition. We also introduced a new simulation technique to assess the quality of the stochastic solution. On the considered instances, the non-convex model provides a commitment that reduces costs (and deficit). Finally, the out-of-sample simulation confirms that the non-convex formulation, combined with the new sustainable proximity measure, is a sound strategy to deal with the SUC problem.

References

- [BCF19] D. Baena, J. Castro, and A. Frangioni. “Stabilized Benders methods for large-scale combinatorial optimization, with application to data privacy”. In: *Management Science* (2019). To appear.
- [Bon+06] J. Bonnans, J. Gilbert, C. Lemaréchal, and C. Sagastizábal. *Numerical Optimization. Theoretical and Practical Aspects*. Universitext. Second edition, xiv+490 pp. Berlin: Springer-Verlag, 2006.
- [Cad10] F. Cadoux. “Computing deep facet-defining disjunctive cuts for mixed-integer programming”. In: *Math. Program.* 122.2, Ser. A (2010), pp. 197–223.
- [DM08] A. L. Diniz and M. E. P. Maceira. “A Four-Dimensional Model of Hydro Generation for the Short-Term Hydrothermal Dispatch Problem Considering Head and Spillage Effects”. In: *IEEE Transactions on Power Systems* 23.3 (Aug. 2008), pp. 1298–1308.
- [Fáb+15] C. Fábian, C. Wolf, A. Koberstein, and L. Suhl. “Risk-Averse Optimization in Two-Stage Stochastic Models: Computational Aspects and a Study”. In: *SIAM Journal on Optimization* 25.1 (2015), pp. 28–52.
- [FFM19] G. L. M. Fredo, E. C. Finardi, and V. L. de Matos. “Assessing solution quality and computational performance in the long-term generation scheduling problem considering different hydro production function approaches”. In: *Renewable Energy* 131 (2019), pp. 45–54.
- [FS13] E. C. Finardi and M. R. Scuzziato. “Hydro unit commitment and loading problem for day-ahead operation planning problem”. In: *International Journal of Electrical Power & Energy Systems* 44.1 (2013), pp. 7–16.

- [FSZ10] M. Fischetti, D. Salvagnin, and A. Zanette. “A note on the selection of Benders’ cuts”. In: *Mathematical Programming* 124.1 (July 2010), pp. 175–182.
- [Geo72] A. M. Geoffrion. “Generalized Benders decomposition”. In: *J. Optimization Theory Appl.* 10 (1972), pp. 237–260.
- [GG74] A. M. Geoffrion and G. W. Graves. “Multicommodity Distribution System Design by Benders Decomposition”. In: *Management Science* 20.5 (1974), pp. 822–844.
- [GH05] A. Gjelsvik and A. Hautstad. “Considering head variations in a linear model for optimal hydro scheduling”. SINTEF Energy Research, Trondheim, Norway. 2005.
- [IBM11] IBM. *IBM ILOG CPLEX Optimizer, High-performance mathematical programming solver for linear programming, mixed integer programming, and quadratic programming*. <http://www-01.ibm.com/software/commerce/optimization/cplex-optimizer/>. 2011.
- [Kau+14] M. Kaut, K. T. Midthun, A. S. Werner, A. Tomasgard, L. Hellemo, and M. Fodstad. “Multi-horizon stochastic programming”. In: *Computational Management Science* 11.1 (Jan. 2014), pp. 179–193.
- [KCW18] C. Kang, C. Chen, and J. Wang. “An Efficient Linearization Method for Long-Term Operation of Cascaded Hydropower Reservoirs”. In: *Water Resources Management* 32.10 (Aug. 2018), pp. 3391–3404.
- [Kiw95] K. C. Kiwiel. “Proximal level bundle methods for convex nondifferentiable optimization, saddle-point problems and variational inequalities”. In: *Mathematical Programming* 69.1 (July 1995), pp. 89–109.
- [KW94] P. Kall and S. W. Wallace. *Stochastic Programming*. John Wiley & Sons, 1994.
- [LTB11] X. Li, A. Tomasgard, and P. I. Barton. “Nonconvex Generalized Benders Decomposition for Stochastic Separable Mixed-Integer Nonlinear Programs”. In: *Journal of Optimization Theory and Applications* 151.3 (July 2011), p. 425.
- [MD77] D. McDaniel and M. Devine. “A Modified Benders’ Partitioning Algorithm for Mixed Integer Programming”. In: *Management Science* 24.3 (1977), pp. 312–319.
- [MOZ17] J. Malick, W. de Oliveira, and S. Zaourar. “Uncontrolled inexact information within bundle methods”. In: *EURO J. Computational Optimization* 5.1-2 (2017), pp. 5–29.
- [MW81] T. L. Magnanti and R. T. Wong. “Accelerating Benders decomposition: algorithmic enhancement and model selection criteria”. In: *Oper. Res.* 29.3 (1981), pp. 464–484.
- [Oli+10] W. Oliveira, C. Sagastizábal, D. Penna, M. Maceira, and J. Damazio. “Optimal scenario tree reduction for stochastic streamflows in power generation planning problems”. In: *Optimization Methods and Software* 25 (6 2010), pp. 917–936.
- [Oli16] W. de Oliveira. “Regularized optimization methods for convex MINLP problems”. In: *TOP* 24.3 (Oct. 2016), pp. 665–692.
- [OS14] W. de Oliveira and C. Sagastizábal. “Level Bundle Methods for Oracles with On-Demand Accuracy”. In: *Optimization Methods and Software* 29.6 (2014).

- [OSS11] W. Oliveira, C. Sagastizábal, and S. Scheimberg. “Inexact Bundle Methods for Two-Stage Stochastic Programming”. In: *SIAM Journal on Optimization* 21 (2 2011), pp. 517–544.
- [PO12] A. Papavasiliou and S. S. Oren. “A stochastic unit commitment model for integrating renewable supply and demand response”. In: *Power and Energy Society General Meeting, 2012 IEEE*. IEEE. 2012, pp. 1–6.
- [PO13] A. Papavasiliou and S. S. Oren. “Multiarea stochastic unit commitment for high wind penetration in a transmission constrained network”. In: *Operations Research* 61.3 (2013), pp. 578–592.
- [Rus86] A. Ruszczyński. “A Regularized Decomposition Method for Minimizing a Sum of Polyhedral Functions”. In: *Mathematical Programming* 35.3 (1986).
- [SF94] G. B. Sheble and G. N. Fahd. “Unit commitment literature synopsis”. In: *IEEE Transactions on Power Systems* 9.1 (1994), pp. 128–135.
- [SS09] R. Sioshansi and W. Short. “Evaluating the impacts of real-time pricing on the usage of wind generation”. In: *IEEE Transactions on Power Systems* 24.2 (2009), pp. 516–524.
- [SZ13] L. M. Silva and R. C. Zambon. “Nonlinearities in Reservoir Operation for Hydropower Production”. In: *World Environmental and Water Resources Congress 2013*. Ed. by C. L. Patterson, S. D. Struck, and D. J. Murray. Cincinnati, Ohio, 2013, pp. 2429–2439.
- [Tah+15] M. Tahanan, W. Van Ackooij, A. Frangioni, and F. Lacalandra. “Large-scale unit commitment under uncertainty”. In: *4OR* 13.2 (2015), pp. 115–171.
- [TTT03] R. H. Tütüncü, K. C. Toh, and M. J. Todd. “Solving semidefinite-quadratic-linear programs using SDPT3”. In: *Mathematical Programming* 95.2 (Feb. 2003), pp. 189–217.
- [WB06] A. Wächter and L. T. Biegler. “On the Implementation of a Primal-Dual Interior Point Filter Line Search Algorithm for Large-Scale Nonlinear Programming”. In: *Mathematical Programming* 106.1 (2006), pp. 25–57.
- [WSL08] J. Wang, M. Shahidehpour, and Z. Li. “Security-constrained unit commitment with volatile wind power generation”. In: *IEEE Transactions on Power Systems* 23.3 (2008), pp. 1319–1327.
- [ZCS17] B. Zhao, A. J. Conejo, and R. Sioshansi. “Unit commitment under gas-supply uncertainty and gas-price variability”. In: *IEEE Transactions on Power Systems* 32.3 (2017), pp. 2394–2405.
- [ZM14] S. Zaourar and J. Malick. “Quadratic stabilization of Benders decomposition”. HALL 01181273 preprint. 2014.
- [ZPR00] G. Zakeri, A. B. Philpott, and D. M. Ryan. “Inexact Cuts in Benders Decomposition”. In: *SIAM J. Optim.* 10.3 (2000), 643–657 (electronic).

Algorithm 4: Stochastic unit-commitment solver (continuation)

10 repeat
11 *Level-bundle descent test*

 Compute f_{lo}^k the optimal value of the 0-1 linear problem

$$\begin{cases} \min & \sum_{i \in \mathbb{I}} \sum_{t \in \mathbb{T}^x} p_t^i \langle \mathcal{F}_t, x_t^i \rangle + \alpha \\ \text{s.t.} & x_t^i \in \mathcal{X}_t(\omega_{[t]}^i) \text{ for all } t \in \mathbb{T}^x, \text{ and } i \in \mathbb{I} \\ & \alpha \geq \mathcal{C}^\ell(x) \text{ for } \ell = 0, \dots, k, \end{cases}$$

 and the bundle gap $\Delta^k := f_{\text{up}}^k - f_{\text{lo}}^k$.

12 If $Fv^k \leq f_{\text{up}}^k - m\Delta^k$, then $\begin{cases} \hat{x}^k = x^k \\ f_{\text{up}}^k = \min(f_{\text{up}}^k, Fv^k) \end{cases}$ [*serious step*]

 Otherwise, set $\hat{x}^k = \hat{x}^{k-1}$ and $f_{\text{up}}^k = f_{\text{up}}^{k-1}$ [*null step*].

13 *Master problem:* Given $\hat{x}^k \in \{0, 1\}^{Nx}$, find (x^{k+1}, α^{k+1}) solving

$$\begin{cases} \min & \sum_{n=1}^{Nx} \left(\frac{1}{2} (x_n + \hat{x}_n^k) - x_n \hat{x}_n^k \right) \\ \text{s.t.} & x_t^i \in \mathcal{X}_t(\omega_{[t]}^i) \text{ for all } t \in \mathbb{T}^x, \text{ and } i \in \mathbb{I} \\ & \alpha \geq \mathcal{C}^\ell(x) \text{ for } \ell = 0, \dots, k, \\ & \sum_{i \in \mathbb{I}} \sum_{t \in \mathbb{T}^x} p_t^i \langle \mathcal{F}_t, x_t^i \rangle + \alpha \leq \kappa f_{\text{lo}}^k + (1 - \kappa) f_{\text{up}}^k. \end{cases} \quad (18)$$

Feasibility check: If the problem above is feasible, let $\mathbf{1b}^{k+1} = f_{\text{up}}^{k+1}$. Otherwise, increase $f_{\text{lo}}^k = \kappa f_{\text{lo}}^k + (1 - \kappa) f_{\text{up}}^k$ and loop line 13 to solve again the *Master program*.

14 *Update:* Set $k = k + 1$.

15 until the gap is sufficiently small: $\mathbf{ub}^k - \mathbf{lb}^k \leq \varepsilon \max(1, |\mathbf{lb}^k|)$ for $k > 0$.

B System details

Below we provide the details about the system considered in the experiments presented in Section 5. As shown in Figure 4, the system has three hydro-plants, each of which having water a reservoir. Table 5 presents the initial, minimum, and maximum volume of the reservoirs of the hydro-plants, and the maximum volume of water spilled per hour. All volumes are in hm^3 . The hydro-plants numbered 1, 2, and 3 have 3, 5, and 4 units, respectively. Units belonging to the same hydro-plant are identical. Table 6 shows the characteristics of the units of each hydro-plant. The second column shows the maximum number of times each unit can be switched on within the time horizon; the third and fourth columns present the minimum and maximum generation of each unit (in MW); and the fifth and sixth columns show the minimum and maximum outflow of each unit (in hm^3). Hydro-plant number 1 is upstream to hydro-plant number number 2 and has one-hour water travel time.

Plant	Initial volume	Minimum volume	Maximum volume	Maximum spillage
1	3129	2283	3340	28600
2	4940	4300	5100	7400
3	5018	1974	5779	6100

Table 5: Characteristics of each hydro-plant.

Plant	Maximum # of start-ups	Minimum generation	Maximum generation	Minimum outflow	Maximum outflow
1	2	0	380	0	437
2	2	0	290	0	320
3	2	0	420	0	344

Table 6: Characteristics of each individual unit of each hydro-plant.

The system has seven thermal units. The details about each thermal unit are displayed in Tables 7 and 8. The first column of each time shows the unit numbers. In Table 7, the second column shows the buses in which the units are located (see Figure 4); the third column presents the start-up costs; the fourth and fifth columns show the minimum and maximum power generation (in MW) of each unit when they are on; the sixth and seventh columns exhibit the ramp-up and -down rates (in MW). In Table 8, the second and third columns show the minimum time (in hours) the units must be on (after they are switched on) and off (after they are switched off), respectively; the fourth column indicates whether the units are on or off at the beginning; while the fifth column informs how long (in hours) they are in that state; and, finally, the last column shows the generation (in MW) of the units at the beginning.

Thermal unit	Bus	Start-up cost	Generation		Ramp rates	
			Minimum	Maximum	Up (δ^+)	Down (δ^-)
1	1	10500	150	485	180	180
2	4	20000	150	470	150	150
3	3	11000	30	130	60	60
4	2	13500	50	170	100	100
5	2	18000	35	87	45	45
6	2	16500	15	50	30	30
7	2	1000	18	55	30	30

Table 7: Characteristics of each thermal unit.

As shown in Figure 4, there are four load demands, located at buses 1, 2, 3, and 4. We have considered the same demand for each scenario. Table 9 presents the demand for each time step at each bus.

The water inflow at time t in plant h is given by

$$\xi_{th}^{\text{inflow}} = \xi_{t-1,h}^{\text{inflow}} \max(0, \zeta + \phi)$$

Thermal unit	Minimum up time	Minimum down time	Initial status	Time on prev. status	Previous generation
1	6	9	on	12	150
2	4	6	on	12	150
3	3	8	off	0	0
4	3	3	on	12	50
5	4	6	off	0	0
6	3	8	off	0	0
7	1	1	off	0	0

Table 8: Characteristics of each thermal unit (continuation).

Time step	Bus				Time step	Bus			
	1	2	3	4		1	2	3	4
1	571	2520	630	337	13	501	3515	584	373
2	529	2333	583	311	14	490	3546	615	334
3	494	2177	545	291	15	463	3334	646	311
4	480	2118	530	283	16	478	2908	675	291
5	497	2191	495	292	17	488	2803	748	260
6	519	2294	485	306	18	624	2721	771	249
7	568	2440	455	334	19	687	2938	792	374
8	605	2568	445	356	20	709	3189	835	438
9	648	2859	442	381	21	669	3323	863	460
10	658	3337	479	417	22	605	3235	876	418
11	626	3442	493	411	23	583	2895	843	374
12	584	3494	501	393	24	551	2807	780	333

Table 9: Demand (MW) at each bus.

where the random variable ζ has a normal distribution with mean 1 and standard deviation 0.025, ϕ has a uniform distribution on the interval $[-0.1, 0.1]$, and $\xi_{0,1}^{\text{inflow}} = 151$, $\xi_{0,2}^{\text{inflow}} = 229$, and $\xi_{0,3}^{\text{inflow}} = 260$. The wind power produced at time t in bus b is given by

$$\xi_{tb}^{\text{wind}} = \begin{cases} \min(0.1\vartheta, \xi_{t-1,b}^{\text{wind}} + 0.05\vartheta\beta), & \text{if this quantity is non-negative,} \\ \xi_{t-1,b}^{\text{wind}}(1 + \varrho), & \text{otherwise,} \end{cases}$$

where ϑ is the average of the total demand, $\xi_{0,b}^{\text{wind}} = 0.05\vartheta$, β has a uniform distribution on the interval $[-1, 1]$, and ϱ has a uniform distribution on the interval $[1, 2]$.